Revisiting the defects structure of MAX phase: the case of Ti4AlN3

Anne Joulain, Ludovic Thilly, Jacques Rabier

Revisiting the defects structure of MAX phase: the case of Ti4AlN3

Journal:	*Philosophical Magazine & Philosophical Magazine Letters*
Manuscript ID:	TPHM-07-Dec-0383.R1
Journal Selection:	Philosophical Magazine
Date Submitted by the Author:	31-Mar-2008
Complete List of Authors:	Joulain, Anne; Université de Poitiers, PHYMAT Thilly, Ludovic; Universite de Poitiers, PHYMAT Rabier, Jacques; Universite de Poitiers-CNRS, PHYMAT
Keywords:	dislocations, microstructural analysis, transmission electron microscopy
Keywords (user supplied):	MAX phases, stacking faults

Revisiting the defects structure of MAX phases: the case of Ti_4AlN_3

A. Joulain, L. Thilly, J. Rabier

PHYMAT, University of Poitiers, 86962 Futuroscope, France

Abstract

Microstructural study of as-grown Ti_4AlN_3 MAX phase has been performed by transmission electron microscopy. Dislocation walls, dislocation nucleation sites and stacking faults are described. In particular, diffraction contrast analysis combined with high resolution images give a new insight into the nature of the stacking faults: contrarily to what is usually postulated, it is shown that the stacking faults possess a shear component in the basal plane. The stacking faults are created by the insertion of MX layers in the lattice via diffusion mechanisms. Their possible role on the deformation mechanism of MAX phases is discussed.

Keywords: MAX phases, dislocations, stacking faults, microstructural analysis, transmission electron microscopy

Introduction

After their discovery in the late sixties, the MAX phases have been recently reconsidered and subjected to tremendous studies from the synthesis and the characterization points of view because of their unique properties, combining the best of metals (machinability, stiffness, electrical and thermal conductivities) and ceramics (damage tolerance, temperature resistance), as reviewed by Barsoum [1]. From the mechanical viewpoint, they are generally brittle at low temperature, i.e. below their Brittle-to-Ductile Transition (BDT) temperature which lies between 800°C and 1000°C. The deformation mode is attributed to a dislocation-

based model involving kink and shear bands and delamination [2-5] leading to Kinking Nonlinear Elastic (KNE) properties [6]. Concerning the deformation microstructure, most of the studies were devoted to the model material Ti_3SiC_2. The major feature of the deformed microstructure is the observation of perfect dislocations confined in the basal (0001) plane because of the very anisotropic laminated structure of the MAX phases. The dislocations may either slip in a single basal plane and are then arranged in arrays or are superimposed in successive basal planes forming walls [1, 2, 5, 7].

Stacking Faults (SFs) are observed in numerous M-A-X systems such as Ti-Si-C, Ti-Al-C, Ti-Al-N, Ta-Al-C and Zr-Al-C [7]. They are attributed to stacking errors in the layers sequence during the synthesis [2], i.e. to a lack of A layer [4] or to an insertion of one or several MX layers [8]. Farber *et al.* proposed an associated fault vector perpendicular to the basal plane, i.e. parallel to the [0001] direction [2]. In that case, SFs should not be involved in deformation mechanisms based on shear by perfect dislocations gliding in the basal planes. From crystallographic arguments, Yu and co-workers have suggested that stacking errors in the layers sequence imply that the fault vector must have a component in the basal plane [8]. However no experimental evidence of this in-plane component was obtained.

Since it is of crucial importance to have a full knowledge of the defects structure to understand the deformation mechanisms and to relate them to macroscopic features such as the brittle or ductile behaviour, the complete characterization of observed defects in as-grown material is necessary.

In this paper, transmission electron microscopy (TEM) was performed on as-grown Ti_4AlN_3 [9-11], one member of the M_4AX_3 family that contains also Ti_4SiC_3 [12, 13] and Ta_4AlC_3 [14]. In the first part, general features of the microstructure are described: dislocations, dislocation nucleation sites and SFs. The second part is devoted to SFs detailed analysis by high resolution transmission electron microscopy (HRTEM) and diffraction contrast analysis.

Finally, the results are discussed and compared to literature data on MAX phases and other nanolaminated materials.

Experimental details

Polycrystalline Ti_4AlN_3 bulk samples were fabricated by hot isostatic pressing with stoichiometry shown to be $Ti_4AlN_{3-\delta}$ (where $\delta = 0.1$) [9-11]. The structure was characterized by X-ray diffraction to confirm the $P6_3/mmc$ symmetry and the residual presence of TiN as initially shown in [10].

Thin foils were prepared by a slow mechanical polishing down to 20µm prior to being argon ion thinned with a Precision Ion Polishing System (PIPS) from GATAN. Conventional TEM study was conducted on a JEOL 200CX microscope operating at 200 kV and HRTEM imaging was performed using a JEOL 3010 microscope operating at 300 kV.

Results and discussion

1) General features

Figures 1a-b-c show weak-beam images of dislocations in a grain whose c-axis lies in the thin foil plane (in these figures, the thin foil has been tilted so the c-axis is not in the figure plane). The dislocations can be divided in two types. First, after studying the thin foil in several crystallographic orientations, parallel dislocations are observed to lie in successive basal planes forming a wall in the $(0\ 1\ \bar{1}\ 0)$ plane. Tilting the sample allows observing the dislocation wall edge on (figure 1d) and determining the dislocation line to be parallel to $[2\ \bar{1}\ \bar{1}\ 0]$. The distance between two successive dislocations is about 0.07µm. These dislocation configurations exhibit two different contrasts (figure 1b) suggesting that they are built with two sets of dislocations with different Burgers vectors which were not possible to be

determined. Inside the wall, interactions between dislocations lying in different basal planes are observed (figure 1b). Such interactions confirm the occurrence of different Burgers vectors; it also implies that the evidenced small segments of dislocation junctions are out of the basal plane.

Secondly, dislocation networks are observed outside of the walls (figure 1c). These networks present some segments that can not lie in the basal plane for geometrical reasons (indicated by white arrows on figure 1a). Isolated dislocations are also observed in the matrix (figure 1a and 1d). Some of them are lying in the basal plane but again some are out of the (0001) plane (indicated by black arrows on figure 1a and 1d).

Figures 2a-b show dislocation loop nucleation sites observed in two different grains. On figure 2a, the nucleated dislocations are perfect and exhibit long segments parallel to [1 $\bar{2}$ 1 0]. Figure 2b shows a dissociated dislocation nucleation site: in the chosen diffraction conditions, the characteristic fringe contrast of planar defects is observed between partial dislocations. In both cases, the exact nature of the nucleation sites is not resolved; in particular, it is not possible to discriminate if they are cavities or inclusions, such as TiN inclusions.

On figure 3a, extended SFs are observed to cross a large Ti_4AlN_3 grain. Different faults exhibit different contrasts in same diffracting conditions (figure 3b) and the contrast is not uniform along a given fault (figure 3c). These observations allow concluding that different fault vectors exist in the structure as well as partial dislocation bonding SFs. A unique SF perpendicular to the basal plane with bounding partial dislocations is also observed (white arrow in figure 3a). Changing the diffracting conditions (figure 3d) shows that this

perpendicular SF remains in contrast when all the other defects are out of contrast evidencing another defect vector family.

Some of the here observed defects have been already reported in other MAX phases, in particular in Ti_3SiC_2. One dislocation wall forming a low-angle boundary has been analysed in details with HRTEM by Farber *et al* [15]. From energy considerations, the authors suggest that the wall is constituted with alternating mixed dislocations with two different Burgers vectors. Our work gives further evidence of such succession of two different type of dislocations forming a stable wall.

Concerning the SFs, such defects have also been reported in other systems such as Ti_3SiC_2 [8, 15], or Ta_4AlC_3 [7, 16] as extensively reviewed by Lin and co-workers [7]. Their general properties are similar to the ones observed here in Ti_4AlN_3, i.e. the SFs cross entire grains and lie in the (0001) plane.

As compared to literature, our work evidences numerous new features such as dislocations lying out of basal plane, interacting dislocations (in and out of basal planes), perfect and dissociated dislocation nucleation sites, complex SFs lying in and out of the basal plane. According to these new features, thorough studies (dislocation lines and Burgers vectors, fault vectors and habit planes of the SFs) are needed to shed light on the impact of native defects on deformation mechanisms. In this context what follows is devoted to SFs analysis.

2) revisiting SFs structures

Figure 4a is an HRTEM image of one of the SFs observed in figure 3, figure 4b showing the corresponding Fourier-filtered image. The HRTEM image is obtained with the electron beam parallel to the $[\bar{1}\ 0\ 1\ 0]$ direction, i.e. the SF is observed edge-on. Because the point resolution could not be achieved and due to the phase-contrast imaging of the HRTEM images, the

stacking sequence of the planes along the [0 0 0 1] direction is not trivial without comparison to simulated images using experimental conditions (TEM foil thickness and imaging defocus). Nevertheless, from careful examination of the contrast sequence observed in the non faulted region and comparison with the theoretical lattice structure [11], the TiN planes location can be deduced and enumerated (figure 4): the faulted region consists of the succession of 7 TiN layers in-between 2 Al planes. The observed SF is thus the result of the insertion of 3 extra TiN layers in the Ti_4AlN_3 structure. As a consequence, the SFs lie in the basal plane and the associated fault vectors **R** have a component perpendicular to the habit basal plane, $\mathbf{R}_\perp$.

Figures 5a-b-c-d show planar defects lying in a grain whose (0 0 0 1) plane is almost in the thin foil plane. Images are obtained in two beam dark field conditions with different diffracting vectors **g**. We observe that the defects are actually built with different SFs lying in basal planes and separated by partial dislocations. The different contrasts of the partial dislocations and SFs are reported in table 1. The analysis is here focussed on SFs SF1, SF2, SF3 and SF4, and their bounding partial dislocations d1, d2 and d3. The invisibility rules are used for determining the Burgers vector **b** of dislocations, i.e. $\mathbf{g}.\mathbf{b} = 0$, and the fault vector **R** of SFs, i.e. $\mathbf{g}.\mathbf{R} = 0$ or n where n is an integer.

In the micrograph displayed in figure 5a, all the SFs are in contrast. Figure 5b and 5c are obtained with respectively $\mathbf{g_1}=[1\ \bar{1}\ 0\ 6]$ and $\mathbf{g_2}=[0\ 1\ \bar{1}\ \bar{6}]$. In such conditions, the defects exhibit complementary contrast: SFs that are in contrast in figure 5b, are out of contrast in figure 5c and *vice versa*. Such feature evidences that, first the SFs have different faults vectors and secondly that these fault vectors can not be parallel to the [0 0 0 1] direction: if so, for a given SF, the contrasts would have been identical with both used diffracting vectors $\mathbf{g_1}$ and $\mathbf{g_2}$. Consequently, fault vectors have a component in the basal plane, $\mathbf{R}_{//}$. On figure 5d, obtained with the diffracting vector $\mathbf{g_3}=[1\ \bar{2}\ 1\ 0]$, all SFs are out of contrast while the bounding partial dislocations are in contrast. SFs are also out of contrast with $\mathbf{g_4}=[2\ \bar{1}\ \bar{1}\ 0]$ and $\mathbf{g_5}=[1\ 1\ \bar{2}\ 0]$.

Thus the observed SF contrasts obtained with the 5 different diffracting vectors are consistent with a fault vector containing an in-plane component $\mathbf{R}_{//}$ of 1/3 <0 1 $\bar{1}$ 0> type. In detail, the fault vector $\mathbf{R_1}$ = 1/3 [1 $\bar{1}$ 0 υ_{c1}] for SF1 and SF3 and $\mathbf{R_2}$ = 1/3[0 1 $\bar{1}$ υ_{c2}] for SF2 are indeed in agreement with the observed contrasts ($\mathbf{g_3}.\mathbf{R_1} = 1$, $\mathbf{g_4}.\mathbf{R_1} = 1$, $\mathbf{g_5}.\mathbf{R_1} = 0$; $\mathbf{g_3}.\mathbf{R_2} = -1$, $\mathbf{g_4}.\mathbf{R_2} = 0$, $\mathbf{g_5}.\mathbf{R_2} = 1$). It is worth noting that the component parallel to the *c* axis, υ_c, can not be determined in such experiments: in fact it is likely that this component is not a rational fraction of the *c* parameter. According to contrast analysis, this *c*-component can be written as: n/6 + δ_n. Consistently, we can underline that in figure 5c and 5d, a residual contrast remains for SFs that are considered as "out of contrast". Such residual contrast may be due to the δ_n component.

Concerning the partial dislocations, the observed contrasts allow concluding that they are of two types: dislocations d1 and d3 have a Burgers vector $\mathbf{b_1}$=1/3[0 1 $\bar{1}$ ω_1] (where ω_1 cannot be quantitatively determined here) and dislocation d2 is characterized by a Burgers vector $\mathbf{b_2}$=1/3[1 $\bar{1}$ 0 ω_2].

3) Discussion

Usually, SFs in hexagonal structures proceed from the dissociation in the basal plane of 1/3<1 1 $\bar{2}$ 0> perfect dislocations. In MAX phases, the SFs analysed up to now do not correspond to this scheme: they have been found to be related to a defect of the lamellar structure and present a dilatation component parallel to the *c*-axis, $\mathbf{R}_{\perp}$ [2, 8]. The SFs observed here in Ti_4AlN_3 have as well a dilatation component, but the present analysis gives further details of their nature with the first experimental evidence, in a MAX phase, of an additional in-plane component of the fault vector, $\mathbf{R}_{//}$, as suggested by Yu *et al.* [8]. Previous studies have shown that SFs could correspond to the removal of A planes (Al planes in Ti_4AlN_3) or insertion of

MX layers (TiN layers in Ti_4AlN_3). Here, HRTEM has been used in order to discriminate the second possibility. In Ti_3SiC_2, Yu *et al.* give evidence of the insertion of 1, 3 or 4 TiC layers. In this view, figure 6-a presents the non-faulted Ti_4AlN_3 structure (following the work of Rawn *et al.* [11]) where TiN octahedra are evidenced as well as the prismatic Ti polyhedra in which are nestled the Al atoms. Figure 6-b is a sketch of a faulted structure with the insertion of one extra TiN layer: this insertion leads to the formation of a SF with a $\mathbf{R}_{\perp}$ component. In addition, in order to preserve the local environment of Al atoms, an in-plane component, $\mathbf{R}_{//}$, is necessary. It corresponds to the translation $1/3\langle 0\ 1\ \bar{1}\ 0\rangle$ between the 3 different types of Ti planes (named A, B or C in [1]).

Yu *et al.* show, in the case of Ti_3SiC_2, that the insertion of 1 or 4 TiC layers along [0001] direction requires an identical shear component to be accommodated in the structure whereas the insertion of 3 TiC layers does not necessitate any translation in the basal plane. The SF observed on the figure 4 corresponds to the latter case.

In fact, a SF can be interpreted as an embryo of MX platelet embedded in the MAX matrix (for instance TiC platelet embedded in the Ti_3SiC_2 matrix). Similar planar defects are reported in Ti_2AlC [17] (where even larger TiC platelets are observed in the matrix), in Ti_3AlC_2 [18] or in Tantalum Aluminium carbides (Ta_2AlC, Ta_3AlC_2 and Ta_4AlC_3, where TaC layers are inserted in the matrix [16]). This situation is in some aspect similar to the one observed in the layered superconducting ceramics $YBa_2Cu_3O_{7-\delta}$ (YBCO). In these orthorhombic structures, SFs with $1/6\langle 3\ 0\ 1\rangle$ fault vectors are one of the major features of the as-grown material substructure [19]. These defects result from the insertion of one CuO layer in the matrix as a precursor of the $YBa_2Cu_4O_8$ phase: the associated so-called 'shear component' $1/6\langle 3\ 0\ 0\rangle$ parallel to the basal plane (equivalent to $\mathbf{R}_{//}$ in the present study) allows preserving an energetically favourable atomic configuration [20]. The nucleation of such defects requires diffusion processes and CuO sources. In YBCO, second phase Y_2BaCuO precipitates act as

CuO reservoirs and most of the SFs are observed attached to these particles. In the case of Ti_4AlN_3, residual presence of TiN is evidenced by X-Ray diffraction (about 3vol% TiN remain in the final compound) that could act as TiN reservoir. On contrary to the YBCO superconductors, the SFs are here not observed attached to TiN precipitates. However, the samples are obtained by hot isostatic pressing at 1275K for 24 hours followed by annealing at 1598K for 168 hours in order to reduce the residual presence of TiN. In such processing conditions, diffusion processes may be highly activated allowing precipitation of TiN extra layers in the Ti_4AlN_3 structure. The presence of a majority of SFs crossing entire grains can be seen as a further element to support the hypothesis of the insertion of TiN extra layers (or platelets) via favourable diffusion paths such as grain boundaries.

Concerning the mechanical properties of MAX phases, Barsoum *et al.* proposed a room-temperature plastic deformation mechanism based on shear deformation by easy dislocation glide in the basal plane for well oriented grains (soft grains), and kink band boundaries nucleation and buckling for misoriented grains (hard grains) [2, 5]. This model was supported by observations of room-temperature deformed macro-grained Ti_3SiC_2 samples, where SFs are not reported [5]. As pointed by El-Raghy *et al.* [21], the origin of the BDT transition can be essentially two-fold: (i) an increase of ease of kinking, microcracking and cavity formation [22]; (ii) the activation of non-basal slip system. Despite the lack of experimental observations supporting the second hypothesis, the latter can not be totally ruled out as underlined by Li et al. [23]. Actually, our observation of out-of-basal-plane dislocations in as-grown Ti_4AlN_3 could support this hypothesis. Moreover, the here reported experimental evidence of a shear component of the SF vectors implies to reconsider the role of planar defects in the plastic deformation. Note that defects of this type have been found to allow for stress relaxation in YBCO indented at room temperature [24]. At high temperature where diffusion is more efficient, the contribution of such defects to plasticity is likely to be

enhanced. In this scheme, the role of the residual TiN inclusions, acting as potential sources for TiN extra planes, has also to be considered, as well as the TiN diffusion in the matrix. Of course, TEM observations on Ti_4AlN_3 samples deformed at different temperatures are needed to evaluate the exact role of out-of-basal-plane dislocations and SFs in the deformation mechanisms.

Dislocation nucleation sites are also observed in this work, one of them being associated with partial dislocations. The exact nature of the nucleated SFs remains unknown: it was not experimentally possible to determine whether they correspond to the same SFs as observed elsewhere in the Ti_4AlN_3 matrix or to the classical SFs of the hexagonal structures. The resolution of the nucleation site, that seems to be an inclusion, should give some elements to discriminate both defects. It is worth recalling that the deformation mechanism proposed by Barsoum *et al.* [5] is based on earlier model of Frank and Stroh [25] that proposes kink-band formation as a deformation mechanism of hexagonal metallic single crystals. Actually, Frank and Stroh suggest that cavities or inclusions could act as permanent dislocation nucleation sites allowing for kink-band formation. In this case, emitted dislocations should have opposite signs on both sides of the source. In the Ti_4AlN_3 matrix, the complete identification of the emitted dislocation Burgers vectors, in particular their sign, has to be performed in order to confirm such hypothesis.

4) Summary and conclusion

From complementary diffraction contrast and HRTEM analyses, the as-grown microstructure of Ti_4AlN_3 polycrystalline samples was revisited. Several features are in agreement with literature data on other MAX phases; however, detailed examination of the dislocations networks and SFs contrasts allowed observing original crucial elements:

1- Out-of-basal-plane dislocation segments are observed both in dense walls and in isolated loose networks. Such defects may interact with basal dislocations impeding their movement through tree forest interactions.

2- Perfect dislocation as well as partial dislocation nucleation sites are evidenced. Nucleation events seem to occur at inclusions or cavities.

3- The fault vector **R** of the SFs is not unique and is composed of a shear component in the basal plane, $\mathbf{R}_{//} = 1/3 \langle 0\ 1\ \bar{1}\ 0 \rangle$, and a dilatation component, $\mathbf{R}_{\perp}$, that is most probably not a rational fraction of the c parameter (its proposed value $\upsilon_c = n/6 + \delta_n$ may be related to the nature of the fault in the lattice sequence). It is suggested that the SFs originate from the insertion of extra TiN (MX) layers in the Ti_4AlN_3 structure: these SFs may be created by processes involving diffusion of TiN from reservoirs such as residual TiN inclusions.

4- The SF bounding dislocations are partials with **b** of the $1/3\langle 0\ 1\ -1\ \omega \rangle$ type; ω could not be determined but since its value is non zero, **b** does not belong to the basal plane.

As a conclusion, the present study shows that careful examination of as-grown Ti_4AlN_3 microstructure with diffraction contrast TEM techniques (two-beam or weak-beam conditions) gives new insights into the nature of defects. In particular, contrarily to what is usually postulated in literature, the SFs possess an in-plane component. This shear component could be also present in the dissociation of dislocations. These new elements could shed a new light on the comprehension of plastic deformation mechanism of MAX phases.

Acknowledgements

Prof. Michel W. Barsoum, from Drexel University Philadelphia USA, is acknowledged for providing the Ti_4AlN_3 polycrystalline samples.

References

[1] M. W. Barsoum, Prog. Solid St. Chem. **28** (2000) 201.
[2] L. Farber, M. W. Barsoum, A. Zavaliangos, *et al.*, J. Amer. Cer. Soc. **8** (1998) 1677.
[3] M. W. Barsoum, T. El-Raghy, Met. Mater. Trans. A **30A** (1999) 363.
[4] B. J. Kooi, R. J. Poppen, N. J. M. Carvalho, *et al.*, Acta Mater. **51** (2003) 2859.
[5] M. W. Barsoum, L. Farber, T. El-Raghy, Met. Mater. Trans. A **30A** (1999) 1727.
[6] M. W. Barsoum, T. Zhen, A. Zhou, *et al.*, Phys. Rev. B **71** (2005) 134101.
[7] Z. Lin, M. Li, Y. Zhou, J. Mater. Sci. Technol. **23** (2007) 145.
[8] R. Yu, Q. Zhan, L. L. He, *et al.*, Phil. Mag. Lett. **83** (2003) 325.
[9] A. Procopio, M. W. Barsoum, T. El-Raghy, Met. Mater. Trans. A **31A** (2000) 333.
[10] A. Procopio, T. El-Raghy, M. W. Barsoum, Met. Mater. Trans. A **31A** (2000) 373.
[11] C. J. Rawn, M. W. Barsoum, T. El-Raghy, *et al.*, Mat. Res. Bull. **35** (2000) 1785.
[12] H. Högberg, L. Hultman, J. Emmerlich, *et al.*, Surf. & Coat.Technol. **193** (2005) 6.
[13] M. Magnuson, M. Mattesini, O. Wihelmsson, *et al.*, Phys. Rev. B **74** (2006) 205102.
[14] P. Eklund, J.-P. Palmquist, J. Höwing, *et al.*, Acta Mater. **55** (2007) 4723.
[15] L. Farber, I. Levin, M. W. Barsoum, Phil. Mag. Lett. **79** (1999) 163.
[16] Z. Lin, M. J. Zhuo, Y. Zhou, *et al.*, J. Amer. Cer. Soc. **89** (2006) 3765.
[17] Z. Lin, M. J. Zhuo, Y. Zhou, *et al.*, Acta Mater. **54** (2006) 1009.
[18] X. L. Ma, Y. L. Zhu, X. H. Wang, *et al.*, Phil. Mag. **84** (2004) 2969.
[19] J. Rabier, F. Sandiumenge, J. Plain, *et al.*, Rad. Eff. & Def. in Sol. **157** (2002) 871.
[20] J. Rabier, Phil. Mag. A **73** (1996) 753.
[21] T. El-Raghy, M. W. Barsoum, A. Zavaliangos, *et al.*, J. Amer. Cer. Soc. **82** (1999) 2855.
[22] D. Chen, K. Shirato, M. W. Barsoum, *et al.*, J. Amer. Cer. Soc. **84** (2001) 2914.
[23] J.-F. Li, W. Pan, F. Sato, *et al.*, Acta Mater. **49** (2001) 937.
[24] A. Proult, P. D. Tall, J. Rabier, J. Mater. Sci. **36** (2001) 2451.
[25] F. C. Frank, A. N. Stroh, Proc. Phys. Soc. B **65** (1952) 811.

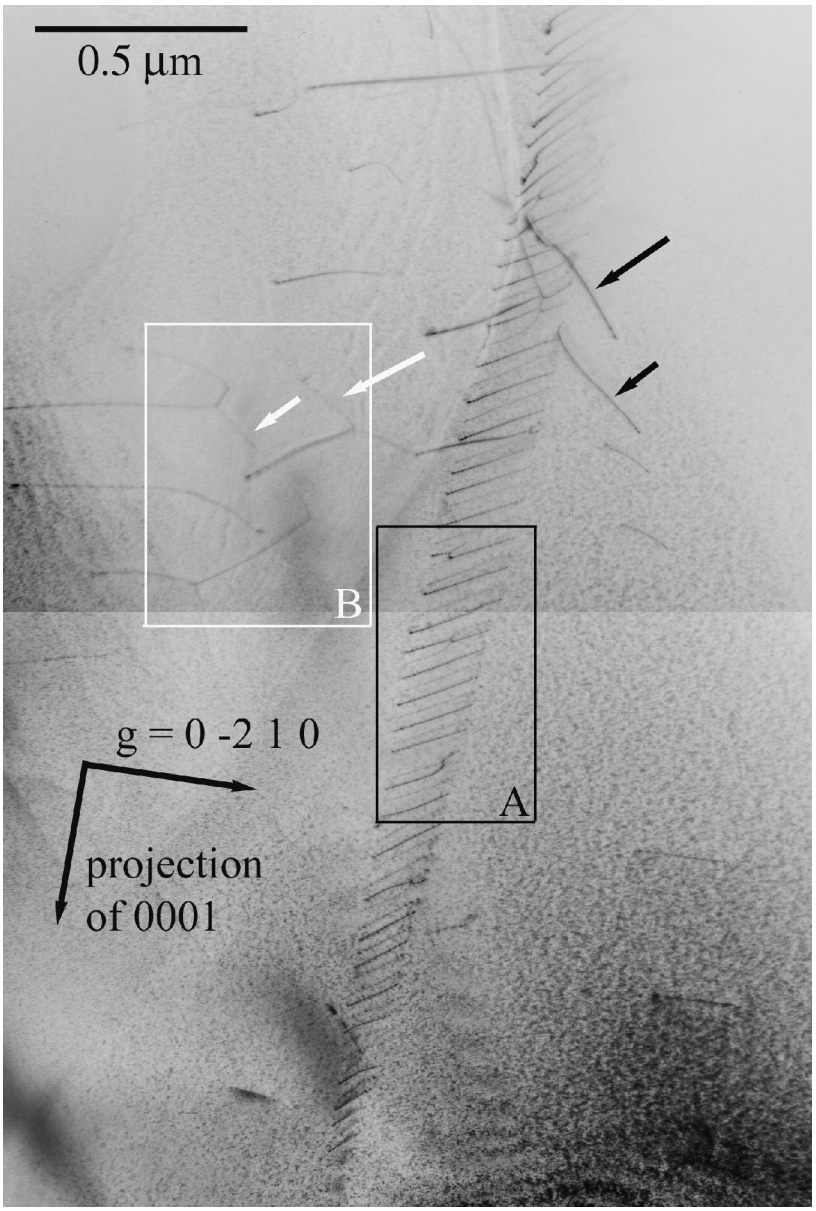

Figure 1a: Weak-beam image of dislocations in a Ti_4AlN_3 grain with c-axis in the thin foil plane. Dislocation networks and dislocation wall parallel to the (0 1 -1 0) plane. White and black arrows point to out-of-basal-plane dislocations.
64x96mm (600 x 600 DPI)

Figure 1b: Zoom-in on region A showing the detailed structure of the wall with successive dislocations exhibiting different contrasts.
17x24mm (600 x 600 DPI)

Figure 1c: Zoom-in on region B revealing dislocation network with out-of-basal-plane segments.
23x30mm (600 x 600 DPI)

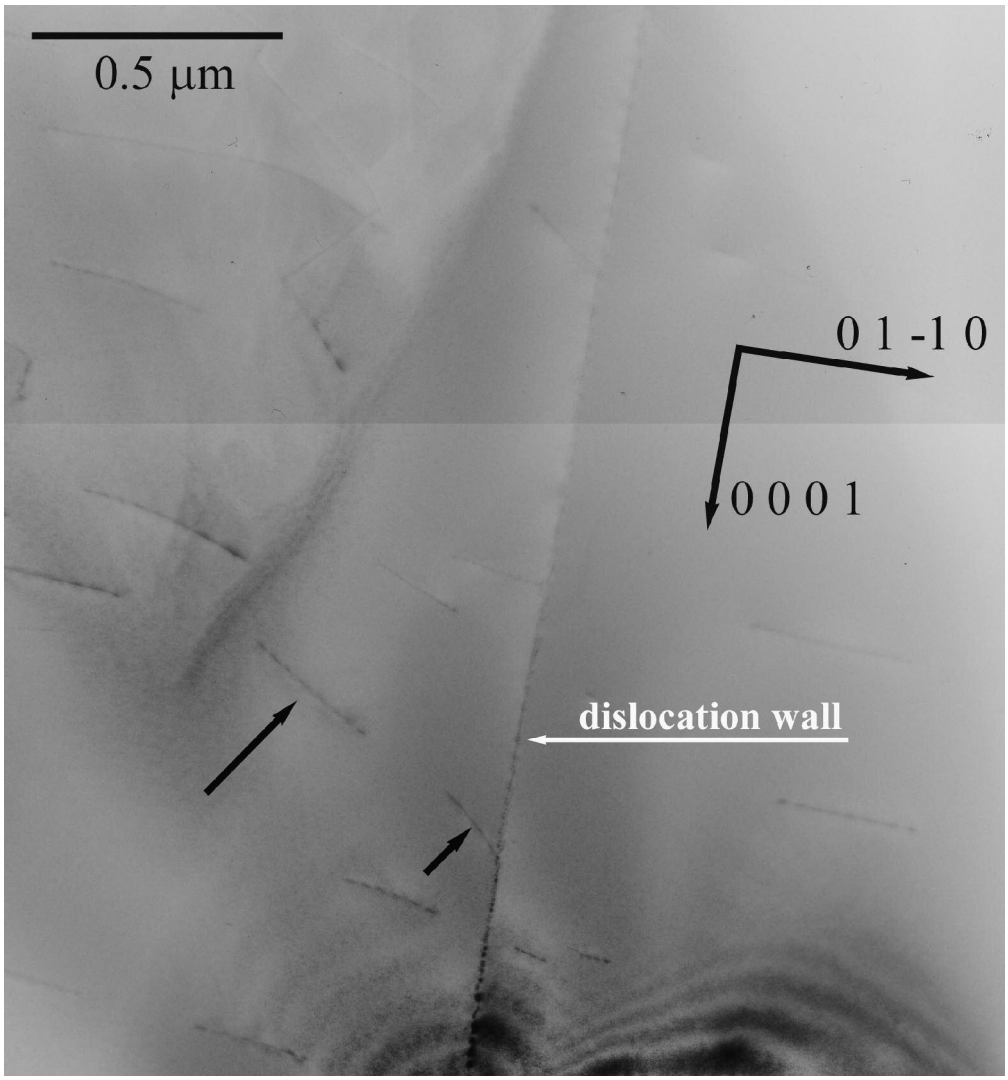

Figure 1d : Dislocation wall observed edge on and isolated dislocations in the matrix. Some of them (indicated by black arrows) are lying out of the basal plane.

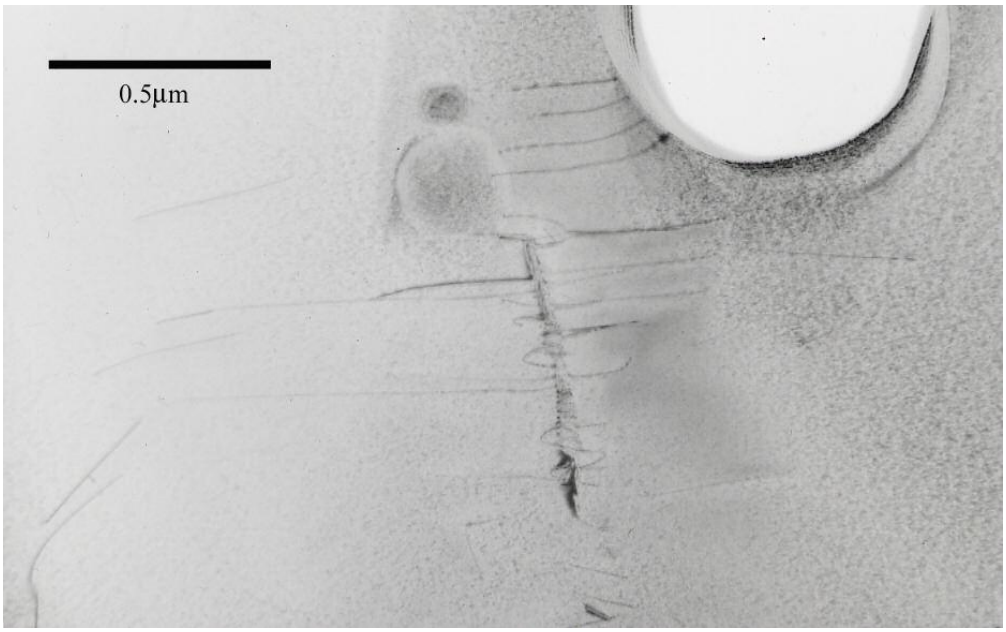

Figure 2a: Perfect dislocation loop nucleation site.
78x49mm (300 x 300 DPI)

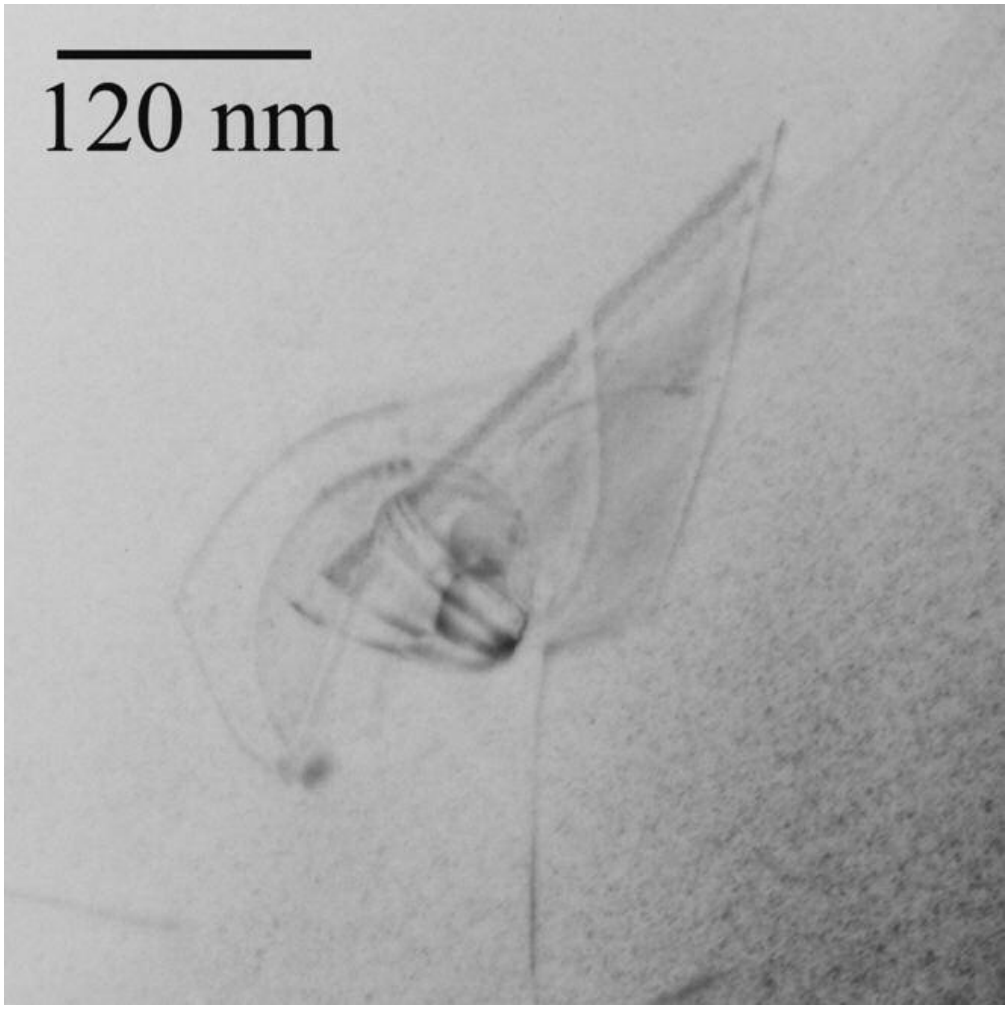

Figure 2b: Partial dislocation loop nucleation site.
27x27mm (600 x 600 DPI)

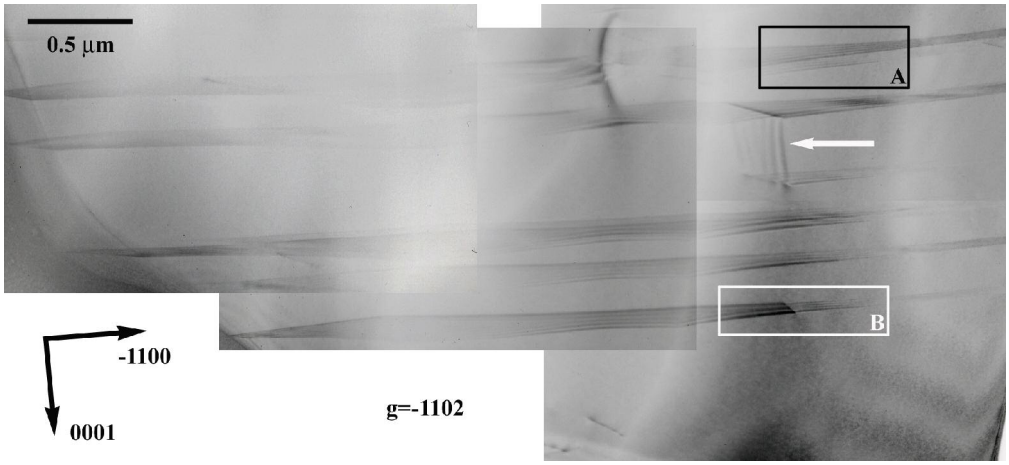

Figure 3a: Stacking faults crossing a large Ti_4AlN_3 grain. The white arrow indicates a stacking fault perpendicular to the basal plane.

Figure 3b: Zoom-in on region A showing two neighbouring stacking faults exhibiting different contrast in same diffracting condition.
9x3mm (600 x 600 DPI)

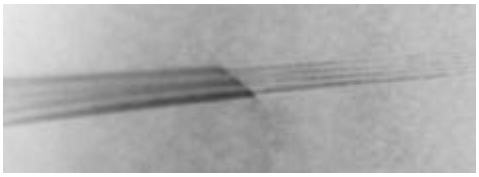

Figure 3c : Zoom-in on region B with a change of contrast along one of the defects. Both parts are separated by a partial dislocation.
9x3mm (600 x 600 DPI)

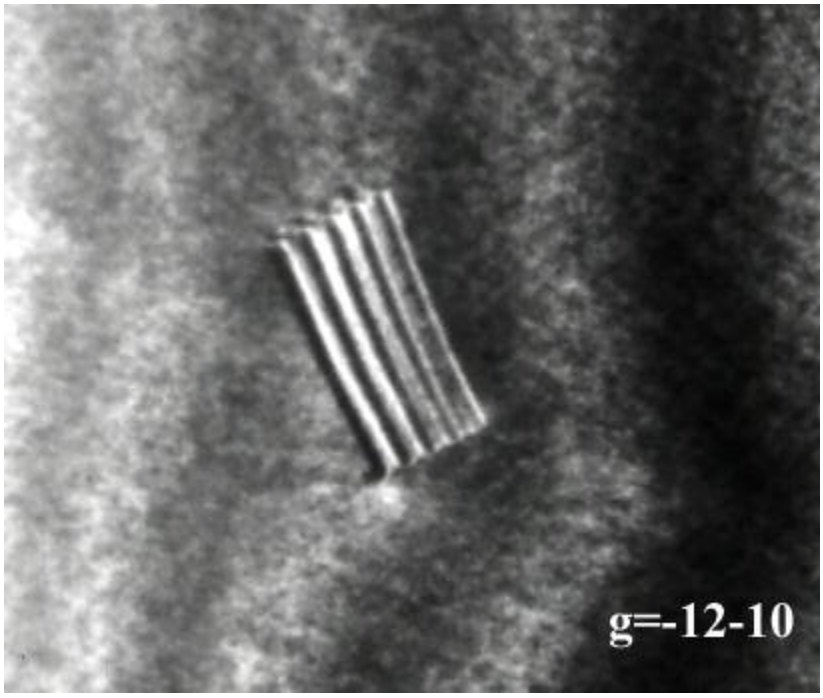

Figure 3d: Stacking fault perpendicular to the basal plane; in the chosen diffracting condition, this defect remains in contrast when all the other stacking faults are out of contrast.
34x29mm (300 x 300 DPI)

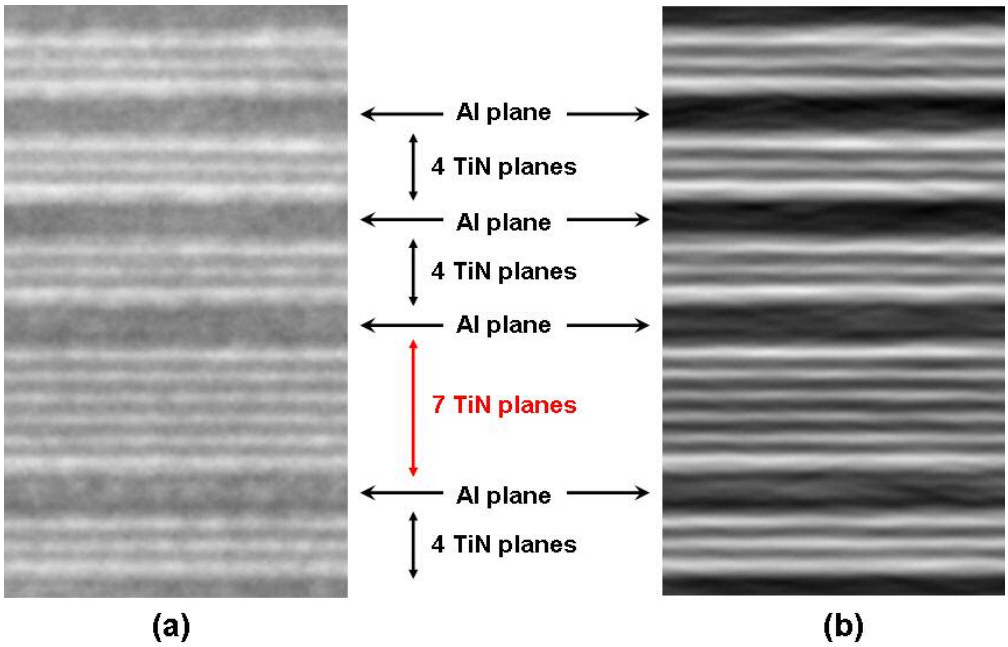

Figure 4 : HRTEM images with associated stacking sequence. (a) Image obtained with the electron beam parallel to the [-1 0 1 0] direction. (b) Corresponding Fourier-filtered image.

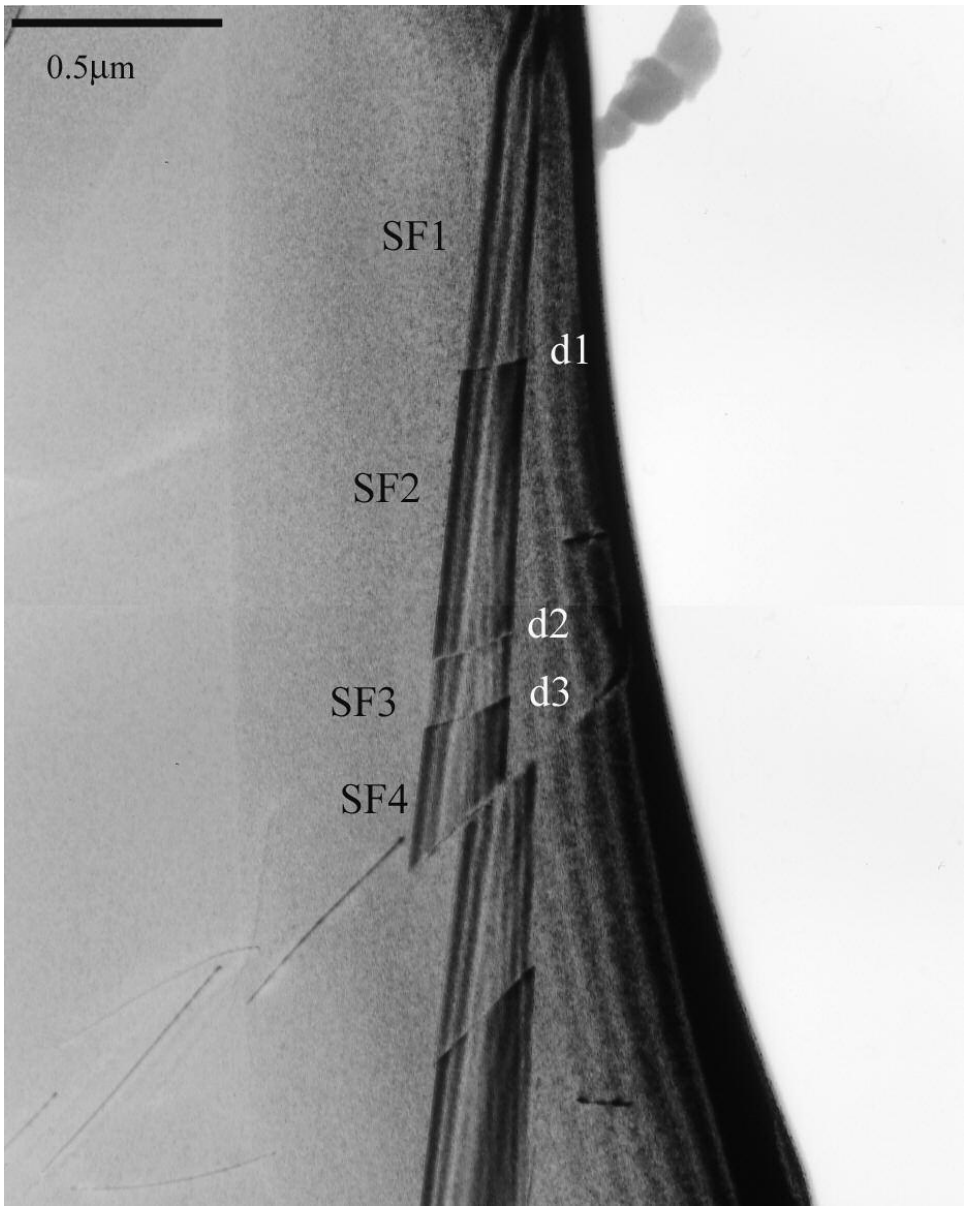

Figure 5a: Planar defects lying in a grain whose (0001) plane is close to the thin foil plane. The defects are constituted with successive stacking faults SFi separated by partial dislocations di.

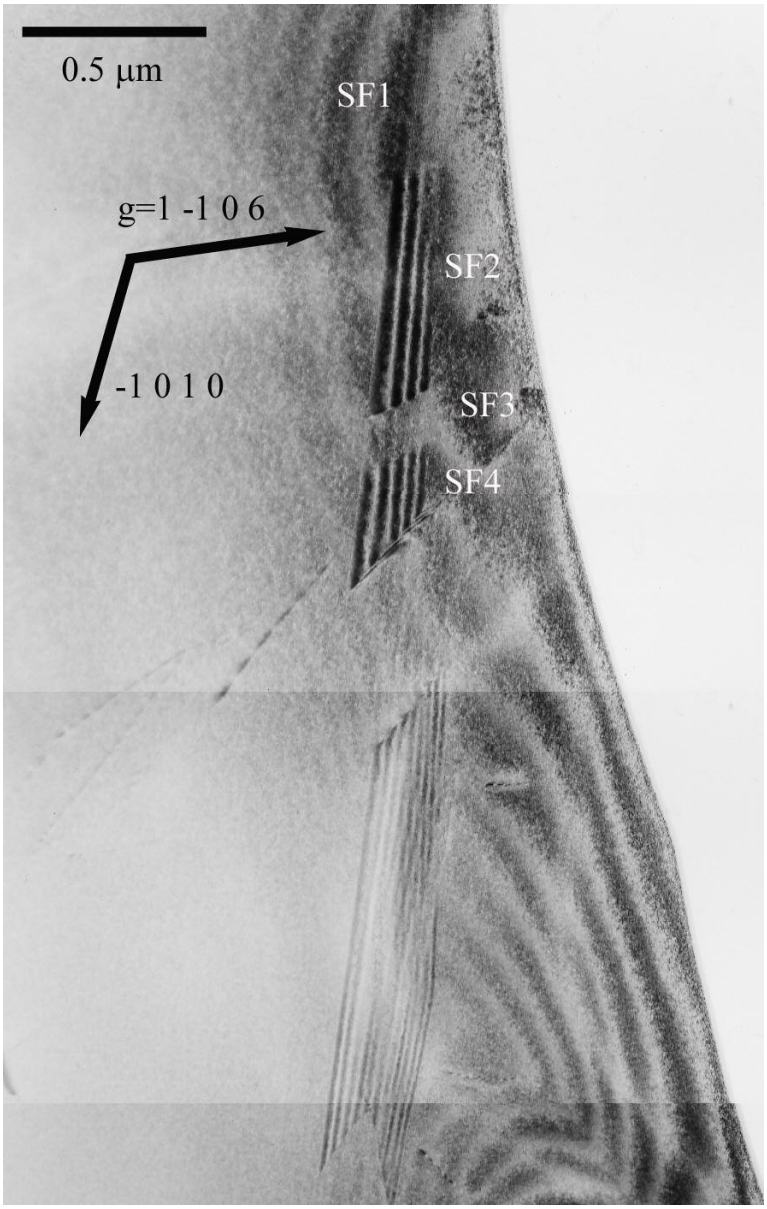

Figure 5b: Planar defects lying in a grain whose (0001) plane is close to the thin foil plane. Stacking faults imaged with g1=[1 -1 0 6].

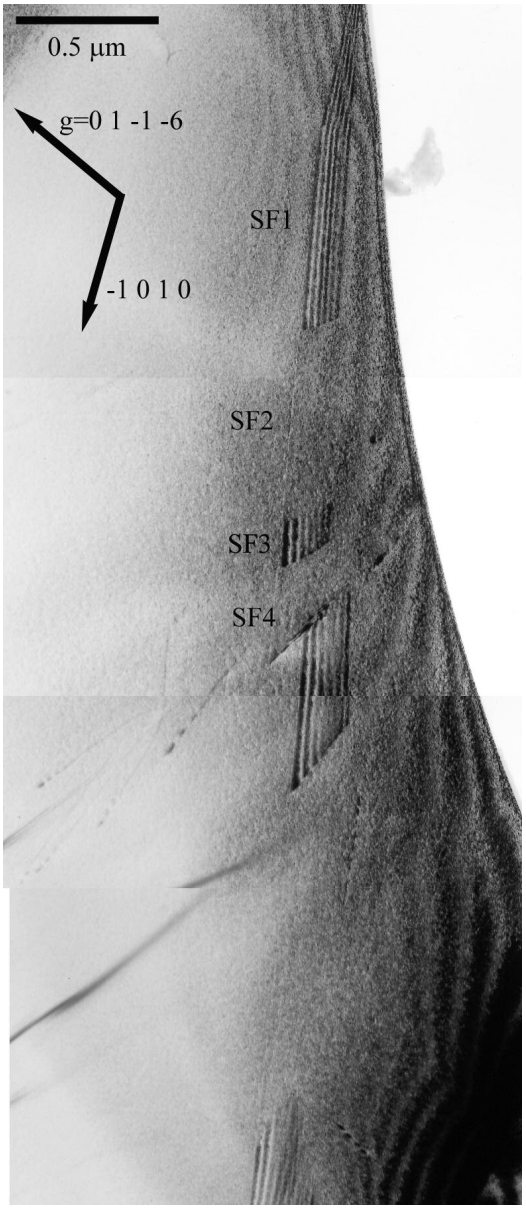

Figure 5c: Planar defects lying in a grain whose (0001) plane is close to the thin foil plane.Stacking faults imaged with g2=[0 1 -1 -6]. The SFs contrast is complementary to the one observed on (b).

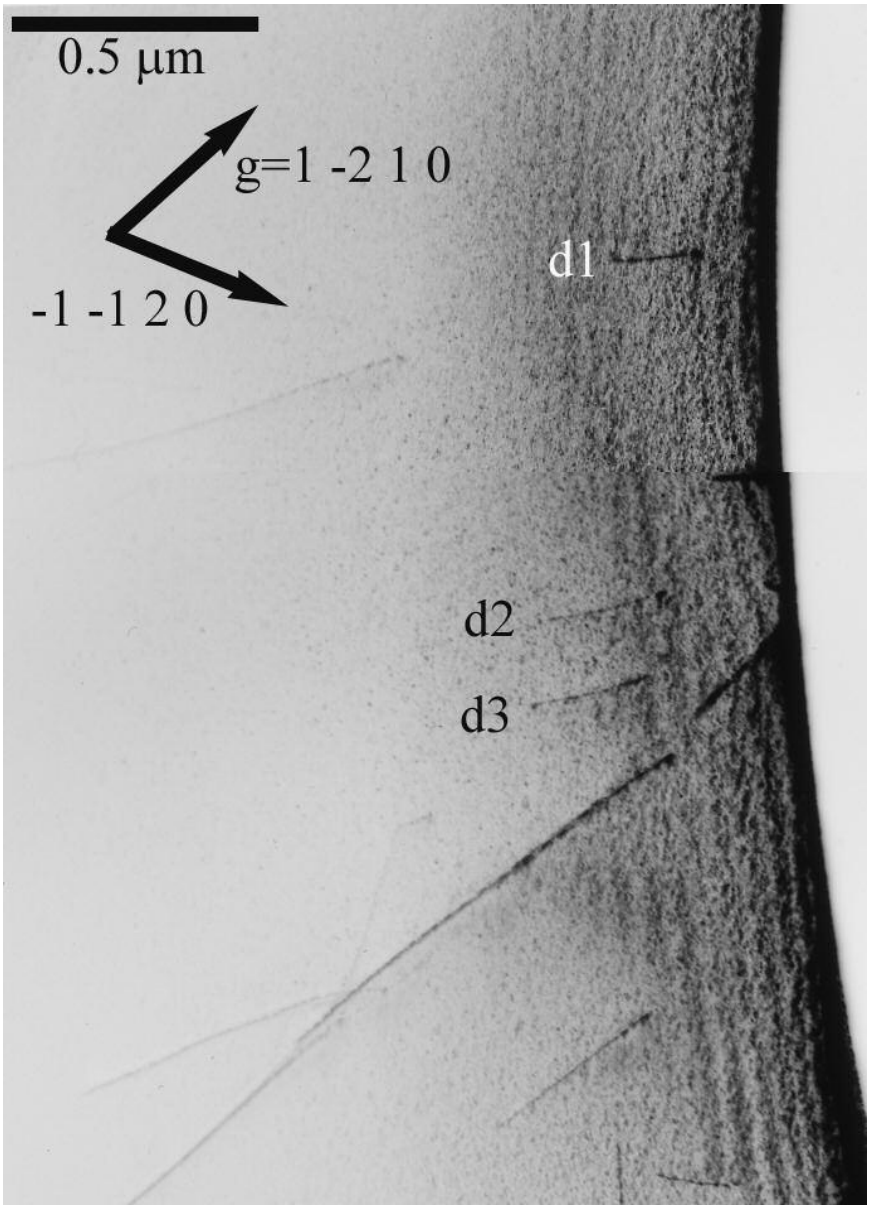

Figure 5d: Image obtained with g3=[1 -2 1 0]; in this condition, all the SFs are out of contrast when partial dislocations are in contrast

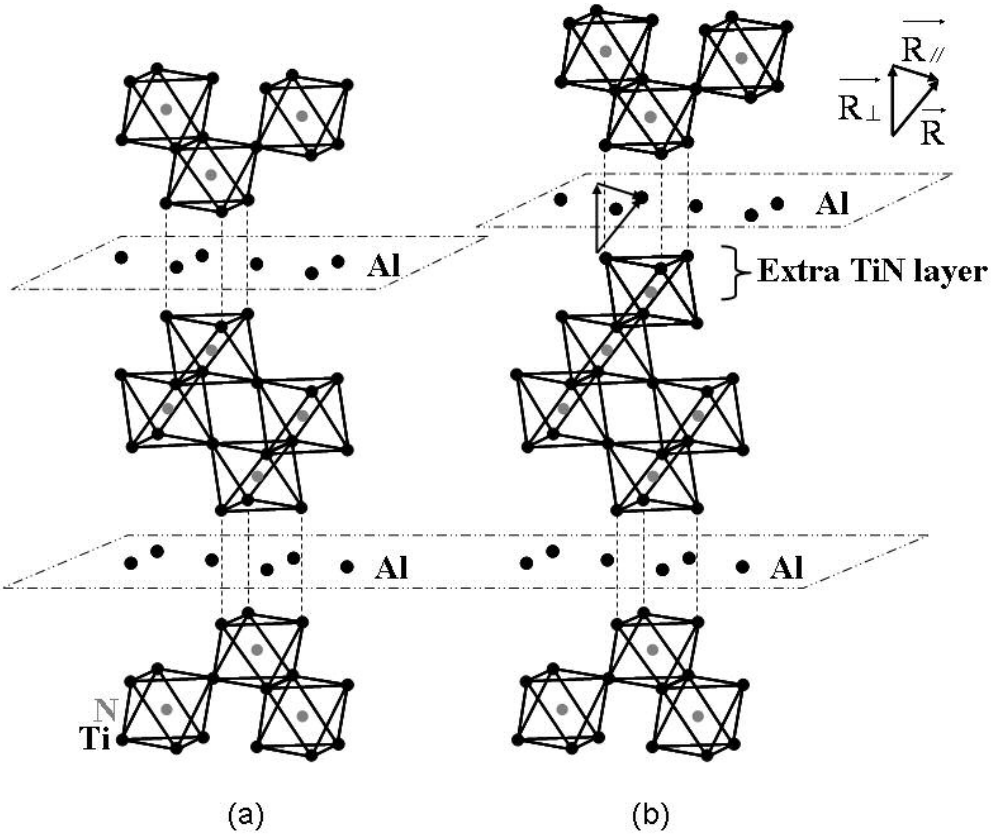

Figure 6 : (a) Crystal structure of Ti_4AlN_3 (from [11]) where TiN octahedra are evidenced as well as the prismatic Ti polyhedra in which are nestled the Al atoms. (b) The faulted structure with the insertion of one TiN layer: this insertion leads to the formation of a SF with a fault vector $R = R_{//} + R_{\perp}$.

Table 1

	$\mathbf{g_1=[1\ \bar{1}\ 0\ 6]}$	$\mathbf{g_2=[0\ 1\ \bar{1}\ \bar{6}]}$	$\mathbf{g_3=[1\ \bar{2}\ 1\ 0]}$	$\mathbf{g_4=[2\ \bar{1}\ \bar{1}\ 0]}$	$\mathbf{g_5=[1\ 1\ \bar{2}\ 0]}$
d1	-	-	in contrast	out of contrast	in contrast
d2	-	-	in contrast	in contrast	out of contrast
d3	-	-	in contrast	out of contrast	in contrast
SF1	out of contrast	in contrast			
SF2	in contrast	out of contrast		out of contrast	
SF3	out of contrast	in contrast			
SF4	in contrast	out of contrast			